Hydrogen loss in *a*-Si:C:H layers induced by MeV ion beam irradiation

E. H. C. Ullersma, P. Ullersma, and F. H. P. M. Habraken
Interface Physics, Debye Institute, Utrecht University, P.O. Box 80 000, NL-3508 TA Utrecht, The Netherlands
(Received 17 August 1999)

Irradiation of hydrogenated amorphous silicon and its alloys with MeV ions causes the formation of hydrogen molecules inside the material in the region where they were originally bonded. In this paper this effect is experimentally detected by making use of double-layer structures consisting of plasma-deposited hydrogenated and deuterated amorphous silicon-carbon (a-$Si_{1-x}C_x$:H) alloys, with various carbon contents. At the same time we use this effect to study the low-temperature transport of hydrogen molecules through this class of materials. We deduce that at temperatures below the temperature of the onset of thermal desorption, hydrogen molecules can migrate through material having $x=0.2$, and escape into the ambient. For smaller values of x the formation of molecules inside the material eventually results in morphological damage of the films. The results indicate that in the process of hydrogen loss from the material during annealing at lower temperatures, the rate-limiting step is the formation of molecules inside the material. The observation of an isotope effect in the extent of the ion-beam-induced hydrogen desorption leads to a modification of an existing model for this process.

I. INTRODUCTION

Elastic recoil detection (ERD) and other high-energy ion-beam analysis methods like Rutherford backscattering spectrometry and nuclear reaction analysis are powerful techniques for quantitative elemental depth profiling of thin layers of material.[1,2] The number of atoms involved in the binary scattering process is negligible compared to the total number of atoms in the material. From this point of view these methods can be regarded as nondestructive. However, the primary particles lose energy on their way through the material, mainly as a result of Coulomb interactions with electrons and nuclei. In typical experimental situations the energy loss of the MeV projectiles is mainly due to the energy transfer to the electrons.[2] This energy transfer may lead to considerable modifications of the material. These modifications are sometimes accompanied by the loss of hydrogen or other elements, which are present in the material under investigation. Successful models for the loss of hydrogen[3–5] imply that H_2 molecules are formed from two diffusing H radicals, created by the high-energy ion passage, in a relatively small volume in the region where they were originally bonded. The molecules created thus may subsequently migrate through the material, and finally escape into the ambient. It is therefore possible to investigate the molecular hydrogen transport mechanism by creating molecules inside a layer on purpose, while measuring the evolving H_2 molecules. This will shed some light on the presence of molecular hydrogen in a-Si:H (Ref. 6) and a-Si:C:H alloys, since it becomes clear in the present work that in some material molecular hydrogen remains once it has been formed; we show how this can be investigated.

The aim of the present work is twofold: to experimentally show that the basic ingredients of models for an ion-beam-induced loss of hydrogen are correct, and to apply the ion-beam-induced, local molecule formation to investigate the structure and hydrogen transport mechanism in a-Si:C:H layers. Since we estimate that the temperature of the material during ion-beam irradiation is lower than the onset temperature of thermal desorption of hydrogen from the considered materials, which is above 300 °C (see Table I),[7,8] we obtain information about the rate-limiting step in the loss of hydrogen during heat treatment.

The presence of H in low-temperature plasma-deposited amorphous silicon and silicon alloys is important, since it enables the application of these materials in optoelectronic devices like solar cells. On the other hand, the presence of hydrogen may be the source of instability in this class of materials.[9] Therefore, an understanding of the behavior of hydrogen in these films may be of great help to understand the instability. Here we report on an investigation of hydrogen in a-Si:C:H layers with C contents of ≈0, 5, 10, and 20 at. %. Although the a-Si:C:H alloy with 20-at. % C is not meaningfully applied in device structures, the study of hydrogen transport in this material helps us to understand the phenomena at lower C concentrations. It has been shown[7,10–12] that a-Si:C:H layers have open volume defects. The defect density increases when hydrogen outdiffusion takes place. The thermally stimulated induced outdiffusion of hydrogen results in desorption spectra which often show

TABLE I. Overview of the samples used. The individual deposited layers have thicknesses of approximately 0.15 μm, and the c-Si substrate is 525 μm thick. The H and D concentrations have been determined using ERD. T_0 represents the onset of the thermal desorption of hydrogen from the layers.

Sample	Structure	H (D) conc. (at. %)	T_0 (°C)
a956	a-Si:D/a-Si:H/c-Si	13	350
a953	a-$Si_{0.95}C_{0.05}$:H/a-$Si_{0.95}C_{0.05}$:D/c-Si	20	350
a950	a-Si:H/a-$Si_{0.9}C_{0.1}$:D/c-Si		
a951	a-$Si_{0.9}C_{0.1}$:H/a-$Si_{0.9}C_{0.1}$:D/c-Si	28	300
a962	a-$Si_{0.8}C_{0.2}$:H/a-$Si_{0.8}C_{0.2}$:D/c-Si	40	400
a964	a-$Si_{0.8}C_{0.2}$:H/a-$Si_{0.8}C_{0.2}$:H:D/c-Si	40	400

two peaks. We have deduced that hydrogen which desorbs at the lowest temperature (the LT peak) must be ascribed to cross-linking of hydrogen atoms in the material, subsequent transport of hydrogen molecules toward the surface without retrapping in the network, and desorption from the surface.[13]

Model for ion-beam-induced H loss

Observations of hydrogen loss induced by high-energy ion beams have been reported by different groups. Work by Möller *et al.* showed H release from *a*-C:H layers.[14] The loss of hydrogen from organic layers and semiconductors was investigated for different beam types by Marée *et al.*[4] Making use of assumptions of Adel *et al.*,[3] Marée *et al.* developed an adequate model to describe the rate and extent of hydrogen loss from these films. This model allows one to estimate the initial elemental constituency of the layers of interest using the concepts of the effective interaction volume, and the cross section for the H_2 forming process. A short description of the model follows here. The primary-beam ion breaks hydrogen bonds with probability P within an effective track radius r_{eff}. We take l as the characteristic distance for a hydrogen atom to diffuse before being bonded again. The hydrogen atoms are either trapped in the material by the dangling bonds predominantly created by the ion beam or recombine with other hydrogen atoms, forming hydrogen molecules. Thus the hydrogen abstraction reaction is second order in the hydrogen concentration. If the molecules can diffuse through the layer they will leave the layer, which reduces the hydrogen concentration in the material under investigation. In the formalism of Marée *et al.*[4] the H concentration, as a function of the incident ion dose ϕ, is given by

$$H(\phi)=\frac{1}{V+(1/H(0)-V)e^{-K\phi}}, \tag{1}$$

where $H(0)$ is the initial hydrogen concentration, $V=\pi r_{\mathrm{eff}}^2 l$ is the effective recombination volume, and

$$K=\frac{P_{\mathrm{rec}}P^2\pi r_{\mathrm{eff}}^2}{\sin\alpha} \tag{2}$$

is the effective molecular release cross section (α is the angle of incidence with the plane of the surface, and P_{rec} is the proportionality constant which describes the rate of recombination to H_2[3]). From Eq. (1), it becomes clear that the hydrogen concentration stabilizes at $1/V$ at a high ion dose. A somewhat different formalism was presented by de Jong *et al.*[5] de Jong *et al.* made an explicit distinction between two processes, i.e., direct recombination of hydrogen and recombination after diffusion. The first process leads to an equation which describes the ion fluence dependence of the remaining H concentration in the material equal to that of Marée *et al.* The second process takes into account that hydrogen radicals may diffuse inside and outside the ion track before recombination or trapping. In the model of Marée *et al.* these distinct two processes are combined into one, but the loss of hydrogen through recombination of hydrogen radicals outside the immediate ion track region is considered to be so small that it can be neglected. Both models do not include the process of hydrogen molecule formation through a reaction of a hydrogen radical and a bonded hydrogen atom. It was suggested by de Jong *et al.* that this may be important. We will present some indications in Sec. III that this latter reaction indeed may be important.

TABLE II. The beam characteristics used in the ERD measurements. Recoil angle $\varphi=37.5°$. The absorber foil thickness is 9.7 μm Mylar. The beam spot is ≈ 0.15 cm^2. α is the angle of incidence with respect to the plane of the surface.

Ion	Energy (MeV)	α	Layer composition of sample	Stopping power at depth 0 (eV cm^2/10^{15})
Si	12.8	26	*a*-Si:H	653
Si	12.8	26	*a*-$Si_{0.8}C_{0.2}$:H	597
Cu	46.0	25	*a*-Si:H	1431
Cu	46.0	25	*a*-$Si_{0.8}C_{0.2}$:H	1305
Ag	43.3	24	*a*-Si:H	1534
Ag	43.3	24	*a*-$Si_{0.8}C_{0.2}$:H	1423

We set up an experiment in which we monitored the hydrogen ERD yield from *a*-Si:C:H films during the measurements while also measuring the hydrogen gas pressure in the vacuum chamber. In this way we directly measured the effusing hydrogen species. The films which were used for the experiments consist of two layers. In one layer the most common hydrogen isotope protium (^{1}H) is present; in the other deuterium (^{2}H,D), or a mix of both is applied. In this way we obtained information on the region of formation of the molecules by monitoring the relative effusion rates of H_2, HD, and D_2. As the molecular diffusion is strongly influenced by the structure of the layers, we use the effusion characteristics of *a*-Si:C:H layers with different C contents to obtain structural information.

II. EXPERIMENT

Ion irradiation and simultaneous ERD measurements were performed using three different types of ion beams on a series of *a*-Si:C:H samples. During the experiment the partial gas pressure of hydrogen was monitored with a Balzers QMG-064 quadrupole mass spectrometer. The time evolution of the hydrogen pressure was compared to that of the H yield in the ERD spectrum. The irradiation and ERD measurements were carried out in one of the chambers of the UHV system OCTOPUS.[15] This chamber has a base pressure in the low 10^{-9}-mbar range, and is connected to the Utrecht 6.5 MV tandem Van de Graaff accelerator. The *a*-Si:C:H layers were grown using a plasma-enhanced chemical-vapor deposition process at a temperature of 250 °C in the deposition system ASTER, described in Ref. 16. The kind of hydrogen isotopes present in the layers were adjusted by the choice of the deposition source gases. The source gases were SiH_4 and CH_4, SiD_4 and CD_4, or SiH_4 and CD_4, to obtain *a*-Si:C:H, *a*-Si:C:D, or *a*-Si:C:H:D films, respectively. In the single isotope layers H(D) is bonded to both Si and C.[13] In all cases the total layer thickness amounted to 0.3 μm.

In Table I an overview of the samples is displayed. In addition, in Table II we show the characteristics of the Si, Cu, and Ag ion beams which were used. The stopping power values have been deduced for the assumed layer compositions from the tabulated values of Ziegler *et al.*[17] The stopping power, presented here for the energy of the ion at the

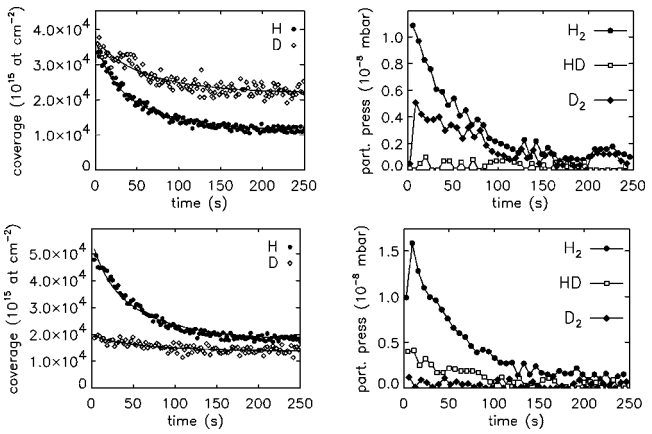

FIG. 1. The change in H and D yields and the H_2, HD, and D_2 partial pressures for 20-at.% C *a*-Si:C:H/*a*-Si:C:D (top) and *a*-Si:C:H/*a*-Si:C:H:D (bottom) samples during 46-MeV Cu ERD measurements. The solid lines in the left figures are fits with Eq. (1).

sample surface, is an important parameter for the temperature rise of the material irradiated. More importantly, the hydrogen loss cross section appeared to depend almost on the square of the stopping power.[4,18] Although it has been verified earlier that the loss of H from the layers is not due to the temperature rise of the material,[4] we have carefully estimated the temperature of the amorphous layers during irradiation, because we want to study the transport of hydrogen through the films to the surface at temperatures lower than the temperature at which thermal desorption of hydrogen commences. The estimation of the temperature is presented in the Appendix. In the Appendix we argue that the temperature in the first seconds after the start of the ion-beam irradiation, where the most important effects are already observed, is of the order of 50 °C or lower.

III. RESULTS AND DISCUSSION

First we concentrate on samples containing 20-at.% C. These samples have initial hydrogen and deuterium concentrations of about 40 at.%. In Fig. 1 we show the H and D abundances in two samples, and the H_2, HD, and D_2 partial pressures during the measurement in the ERD chamber. For this measurement we used a 46-MeV Cu beam at an ion current of about 2×10^{11} particles/s. The samples consist of a 150-nm *a*-Si:C:H layer on top of a 150-nm *a*-Si:C:D or *a*-Si:C:H:D layer. The amount of H in the *a*-Si:C:H/*a*-Si:C:D sample after long irradiation is 30% of the initial amount. In comparison, the D amount is only reduced to 60% of its initial value. One must note that the initial H and D concentrations are equal at the start of the irradiation. The smaller relative amount of the reduction of D compared to H is due to an isotope effect, and not to the fact that the D-containing layer is located below the hydrogenated film, since an inverted structure, i.e., a layer structure in which the deuterium layer is on top, essentially shows the same behavior. The solid lines in the two left parts of Fig. 1 show that both for H and D in both samples an excellent fit with Eq. (1) is possible. The fit parameters are presented in Table III.

The *a*-Si:C:H/*a*-Si:C:H:D sample shows a higher H yield and a lower D yield due to deposition of the bottom layer using SiH_4 and CD_4. The relative decrease in the H yield is comparable to that in the *a*-Si:C:H/*a*-Si:C:D sample; the reduction in the D yield, however, is significantly smaller, 30%. The saturation value for D in this layer is lower than in the *a*-Si:C:H/*a*-Si:C:D sample, which is expected from the presence of H in the bottom layer.

TABLE III. H and D loss data for an experiment with a 46-MeV Cu beam.

Sample	Element	$H(0)$ (10^{18} at. cm^{-2})	$1/V$ (10^{18} at. cm^{-2})	K (10^{-15} cm^2)
*a*962	H	38	11	7.6
*a*962	D	38	22	9.2
*a*964	H	55	17	7.1
*a*964	D	20	14	10.7

The measurements of the partial pressures (Fig. 1) show that H_2 and D_2 molecules evolve from the *a*-Si:C:H/*a*-Si:C:D sample, but nearly no HD molecules are detected. Apparently the molecules are formed inside the distinct layers and are mobile. Because of the spatial separation of incorporated hydrogen and deuterium, only a very limited amount of HD molecules is formed. This confirms the assumption in the model that molecules are formed in a small volume along short segments of the ion track. Consistent with the ERD data, the partial H_2 pressures are larger than the D_2 partial pressures during the ion irradiation, independent of the order of growth of the deuterated and hydrogenated layers.

During the ion irradiation of the sample with the *a*-Si:C:H:D bottom layer, the amount of detected D_2 is very low, the H_2 signal has increased by a factor of 1.5, and the HD signal is clearly present. Comparison of the two cases shows that a layer containing both H and D gives rise to a strong HD signal. This again supports the hypothesis that the molecules are formed close to the place where the individual atoms were bonded initially.

We conclude, therefore, that hydrogen molecules are formed locally under high-energy ion-beam irradiation, and that they are clearly mobile in 20-at.% C *a*-Si:C:H samples at temperatures lower than the onset of the LT thermal desorption spectroscopy peak at 450 °C. At the onset of irradiation of the *a*-Si:C:H/*a*-Si:C:D double-layer structure, the HD gas phase signal is below 5% of the H_2 signal and 10% of the D_2 signal. These observations pose an upper limit to the value of the effective length of diffusion, presumably along the ion track,[4] of about 10–15 nm.

The samples with the lower C concentrations behave differently. In Fig. 2 we show the results of the outdiffusion measurements of the 0-, 5-, and 10-at.% C samples during 43-MeV Ag ion irradiation and simultaneous ERD measurements. The HD and D_2 signals during measurements of the 0- and 5-at.% C are below the detection limit, while the H_2 signal is insignificant in the 0-at.% case and very weak in the 5-at.% C case. In conformity with these observations, the ERD H and D yields show nearly no time or dose dependence. This indicates that either no hydrogen molecules are formed, or that the formed molecules cannot leave the layers. If no hydrogen molecules are formed this would be due to an

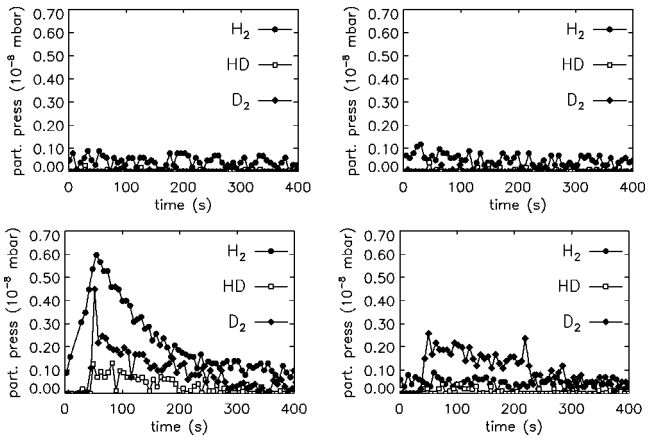

FIG. 2. The H_2, HD, and D_2 partial pressures for *a*-Si:D/*a*-Si:H (top left), *a*-$Si_{0.95}C_{0.05}$:H/*a*-$Si_{0.95}C_{0.05}$:D (top right), *a*-$Si_{0.9}C_{0.1}$:H/*a*-$Si_{0.9}C_{0.1}$:D (bottom left), and *a*-Si:H/*a*-$Si_{0.9}C_{0.1}$:D (bottom right) samples during 43-MeV Ag ERD measurements.

initial hydrogen concentration $[H(0)]$ lower than $1/V$ [Eq. (1)].

The outdiffusion measurement of the 10-at. % C sample shows a gradually increasing H_2 signal and no HD and D_2 signal in the first 40 s. After 40 s the HD and D_2 signals show a sudden increase, followed by a decrease of all signals. The gradual rise indicates that the mobility of the hydrogen molecules is so low that more molecules are formed in a certain time interval than are able leave the layer. Apparently, the D_2 molecules formed in the bottom layer do not even reach the sample surface. A hydrogen pressure builds up in the layer until the layer cracks or is blown away. Then the H_2, HD, and D_2 molecules are released. The formation of a measurable amount of HD molecules may be due to a larger diffusion length or to an enhanced interaction between the H_2 and D_2 molecules in the film that is caused by the longer time of residence of the molecules in the layer.

The effects of cracking of the film and removal of material are clearly shown in the scanning electron microscopy (SEM) recording in Fig. 3. Blisters are formed which crack, leaving craters in the sample surface. Typical diameters of the damage structures are 50 μm. Cross-sectional SEM recordings of cracks showed that the bubbles are formed at

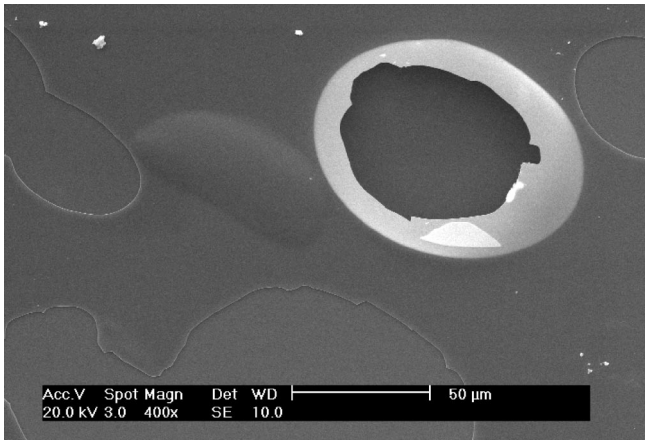

FIG. 3. SEM recording of an *a*-$Si_{0.9}C_{0.1}$:H/*a*-$Si_{0.9}C_{0.1}$:D sample after 43-MeV Ag ERD measurement.

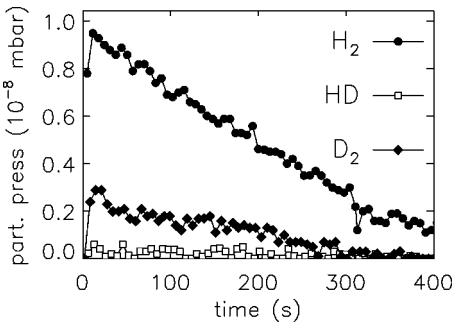

FIG. 4. The H_2, HD, and D_2 partial pressures for an *a*-$Si_{0.8}C_{0.2}$:H/*a*-$Si_{0.8}C_{0.2}$:D sample during 12.8-MeV Si ERD measurements.

depths smaller than the film thickness. This indicates that the cracks are not due to the accumulation of hydrogen molecules at the interface. The reduction of the mobility of the molecules becomes even more clear from the effusion experiment on an *a*-$Si_{0.9}C_{0.1}$:D layer covered by an *a*-Si:H layer (Fig. 2, bottom right). During the first 40 s no outdiffusion is observed; then the layer cracks and the D_2 molecules leave the sample. No significant amounts of H_2 and HD molecules are monitored. This indicates that the H concentration in the *a*-Si:H layer is below the critical concentration for molecule formation, but also that the device-quality *a*-Si:H is not permeable for molecular hydrogen. This implies that once these H_2 molecules have been formed in not too large concentrations, they will remain in the material at moderate temperatures.

In Fig. 4 we show the effusion data of an *a*-$Si_{0.8}C_{0.2}$:H/*a*-$Si_{0.8}C_{0.2}$:D layer recorded during a 12.8-MeV Si ERD measurement. The signal shows a more gradual decrease than in the case of the experiments with the Cu and Ag beams. This is due to the lower stopping power in the film, as shown in Fig. 5. The layers with lower C contents did not show a measurable outdiffusion, where we must keep in mind that the concentrations of H and D are lower in the lower C content samples (Table I).

Isotope effects

Can we learn something from the observation that the extent of D loss from the films compared to that of H is

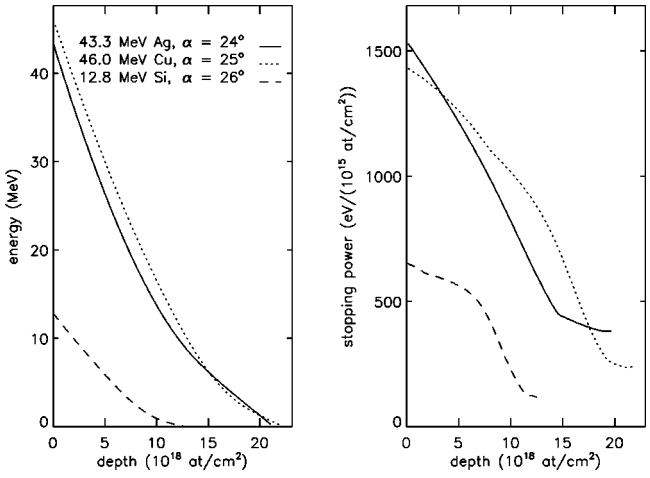

FIG. 5. The energy of the analyzing ion and the stopping power as a function of depth for three different ion beams.

smaller, i.e., that there is a significant isotope effect in the hydrogen loss as a result of ion-beam irradiation? Let us first consider the distinct processes which lead to the disappearance of hydrogen from the layers during ion-beam bombardment. According to the models the first step is the production of atomic hydrogen (deuterium) as a result of decomposition of Si-H and C-H (or Si-D and C-D) bonds. This is assumed to be an electronic process: the ion passage causes a track of ionization events, resulting in breaking of bonds. The resulting H atoms are very reactive; they can react with each other to form a (desorbing) molecule, or they can be trapped into the network and become immobilized. The formation of diffusing and desorbing molecules has been shown in the present work. The relaxation of the electronic system to a ground state is supposed to be fast enough, such that diffusion and chemical reactions take place in an electronically relaxed system. (In the ion track this ground state may very well be different from that before the ion passage.) Finally, when the H (D) concentration has become so low that the probability for a H or D atom to become trapped is much larger than that for the formation of a molecule, the rate of H loss approaches zero.

In the first approximation the electronic processes are not expected to be influenced by isotope effects. The effective radius of the ion track depends on the ionization potential of the hydrogen-containing groups, and will therefore be different for Si-H and C-H groups. We have deduced earlier[13] that in double layers the distribution of H and D over the distinct bonding configurations is similar for the hydrogenated and deuterated layers. In this view, the extent of production of D atoms in the completely deuterated layer, and that of H atoms in the completely hydrogenated layer by the passage of the ion are equal.

The vibrational properties of the hydrogenated groups (SiH_n,CH_n) differ from those of the deuterated groups (SiD_n,CD_n). For instance, the zero-point vibrational energy of Si-H is about 0.05 eV larger than that of Si-D, giving rise to a slightly smaller binding energy for Si-H. The vibration frequency (also called the attempt-to-escape frequency) is a factor of 1.39 smaller in Si-D than in Si-H. For C-H bonds the values are somewhat different, but of the same order of magnitude. This results in a slower rate of decomposition reactions when D is involved in comparison with H. Therefore, the observation of the smaller loss of D, in comparison to H, and the consistent appearance of a smaller D_2 signal in comparison with the H_2 gas phase signal (Fig. 1) point to a significant contribution to the hydrogen loss of these decomposition reactions. This contribution is not included in the current models. In the models the formation of desorbing molecules competes with the process of trapping of atomic H (D), and, at first sight, no decomposition reaction plays a role in these steps of the process.

It is tempting to bring into the discussion the recently observed and discussed isotope effects in the electron- and UV-radiation-induced desorption of hydrogen in Si-H and deuterium in Si-D bonds, adsorbed on Si surfaces, at the SiO_2/Si interface or in GaAs.[19–21] For, as in the work of Foley *et al.* using a scanning tunneling microscope,[19] we are dealing with the interaction of Si-H (Si-D) bonds with low-energy electrons, which in our case are emitted in the primary track by the passing ion. However, in our case we calculate that we lose one bonded H atom per 1–10 electrons, emitted in the track, whereas one apparently needs 10^5–10^6 electrons to stimulate hydrogen or deuterium desorption from a Si-surface.[19] Therefore, we think that this type of isotope effect, which is attributed to the longer lifetime of a vibrationally excited Si-H bond, in comparison to that of a Si-D bond,[19,20,22] does not play a significant role in our case.

One way to proceed is to hypothesize that the formation of a H_2 or D_2 molecule does not occur solely via a reaction with two free atoms, but also via a reaction of a free H (D) atom (radical) and a bonded H (D) atom, resulting, apart from the molecule, in a Si or C dangling bond. The possibility of this hydrogen abstraction reaction was argued by de Jong *et al.*[5] and Maas.[23] In fact, it was reported that the reaction probability between H, chemisorbed on a Si surface in a Si-H bond, and a gas-phase H radical has a value close to unity at 300 °C,[24] and a low activation energy of 0.1 eV.[25] Therefore it is reasonable to attribute the isotope effect to the significant contribution to the hydrogen loss of the reaction $Si\text{-}H + H\cdot \rightarrow H_2 + Si\cdot$. Here $Si\cdot$ denotes a Si with a dangling bond, and $H\cdot$ a hydrogen radical. Similar reactions may occur with CH_n groups.

In the mixed hydrogenated/deuterated layer, hydrogen is mainly bonded to Si, and deuterium to C (see Ref. 13), and hence one might expect a difference in track radius for H and D, in the sense that the group with the largest ionization potential has the smallest effective ion track radius. Therefore, this type of hydrogen bond exhibits the lowest loss rate. This is indeed the case: the Si-H type bonds in general have a smaller ionization potential,[26] and therefore the H loss rate is far greater than the D loss rate. Consistent with the above reasoning, the D_2 signal in the gas phase appears to be low: see Fig. 1. We interpret this to be the result of the low rate of the reaction $C\text{-}D + D\cdot \rightarrow D_2 + C\cdot$. We conclude that the isotope effect on the extent and rate of hydrogen loss in hydrogenated and deuterated amorphous silicon-carbon alloy stacks during MeV ion-beam irradiation can be accounted for, but the existing models to describe this loss must be modified. Thus it is not straightforward to discuss the meaning of the values for K and V [Eq. (1)] obtained from the fits (see Table III). The hydrogen abstraction reaction is second order in the hydrogen concentration; therefore, this essential feature of the models is applicable in the investigated system. A modified model is being developed.[27]

IV. CONCLUSION

The combined measurements of the ERD yield and the desorption products showed that during high-energy ion-beam irradiation of hydrogenated *a*-Si:C:H films, hydrogen molecules are formed close to the position where the H atoms were bonded to the matrix. In samples with an open structure the molecules leave the sample on a time scale of the order of seconds or less. We thus have shown how the nondestructiveness of MeV ion-beam techniques, i.e., the property that two subsequent analyses of the same piece of material gives the same result, only applies for samples having a H concentration below the critical value. By this critical concentration we mean a hydrogen concentration which is asymptotically reached at large fluences and whose value

depends, among other things, on the stopping power of the ions used.[4] From our estimates of the sample temperature we deduce that molecular hydrogen transport takes place at temperatures near room temperature, i.e., below 50 °C. Above that, samples with hydrogen concentrations higher than the critical value, and which are not permeable for H_2, become morphologically damaged during ion-beam irradiation. This is due to the buildup of a large pressure as a result of H_2 formation, which in turn results in the removal of film flakes with typical diameters of 50 μm. We suggest that the presence of molecular hydrogen in material which is not permeable for H_2 at moderate temperatures, as we have shown to be the case for *a*-Si:H and *a*-Si:C:H with low carbon contents, is a source of instability without ion-beam irradiation also. In those circumstances the damage is not macroscopically visible.

From the present results we conclude that in the process of hydrogen loss from the material during annealing at the lower temperatures [i.e., the LT H_2 desorption peak at $300 < T < 450$ °C (Ref. 8)] the rate-limiting step is the formation of hydrogen molecules inside the material, since transport already occurs at lower temperatures. The observed isotope effect in the ion-beam-induced hydrogen loss points to the significant role of thermal decomposition reactions in the hydrogen loss mechanism, which involve the Si-H (Si-D) and/or C-H (C-D) vibrational system.

ACKNOWLEDGMENTS

We acknowledge the crew of the accelerator department, J. Bakker and W. M. Arnoldbik, for help with the experiments, W. F. van der Weg for helpful discussions, and W. G. J. H. M. van Sark for depositing the layers.

APPENDIX A: SAMPLE TEMPERATURE DURING ION IRRADIATION

The energy of ions in an analyzing beam is transformed into heat in the sample under investigation. As argued in Sec. II, we need an estimate of the concomitant temperature rise. To take into account the effect of heat conduction in the sample and its holder, we will consider three models.

In the first model [(a) a semi-infinite solid] it is assumed that the sample is semi-infinite, that the beam spot size is equal to the sample area, that all heat is absorbed at the surface and that no heat is reemitted. Consequently the heat conduction is one dimensional.

The second model [(b) a two-component semi-infinite solid] is a refinement of the first one, in which we take into account the presence of a sample holder made of stainless steel. The sample and sample holder combination is represented by a silicon layer, with the thickness of the sample (0.055 cm) on top of stainless steel. Furthermore, at the boundary between the sample and the holder thermal resistance is taken into account.

In the third model [(c) a lateral model] we describe how absorbed energy flows in an infinitely extended plane of the sample. This represents the actual situation in which the beam spot size is smaller than the area of the sample. The energy is generated within a disk with the size of the beam spot. Consequently, the heat conduction is two dimensional.

The equation of heat conduction for the three models is solved by applying the method of Laplace transformation (cf. Carslaw and Jaeger[28]). We will give the resulting expressions for the energy flux, the temperature profile, and the global temperature rise of the sample (spatial average of the temperature) as a function of time. Furthermore, the influence of the thermal resistance in model (b) is addressed.

Thermal conductivity, difussivity, capacity, and the density of silicon and stainless steel are indicated by $k_{1,2}$, $\kappa_{1,2}$, $c_{1,2}$, and $\rho_{1,2}$. These quantities are related by the equation

$$\kappa_{1,2} = \frac{k_{1,2}}{\rho_{1,2} c_{1,2}}. \tag{A1}$$

The following numerical values were used for the calculations: $k_1 = 1.49\ \mathrm{J\,s^{-1}\,cm^{-1}\,K^{-1}}$, $k_2 = 0.3\ \mathrm{J\,s^{-1}\,cm^{-1}\,K^{-1}}$, $\rho_1 = 2.33\ \mathrm{g\,cm^{-3}}$, $\rho_2 = 8.02\ \mathrm{g\,cm^{-3}}$, $c_1 = 0.705\ \mathrm{J\,g^{-1}\,K^{-1}}$, $c_2 = 0.449\ \mathrm{J\,g^{-1}\,K^{-1}}$ $\kappa_1 = 0.91\ \mathrm{cm^2\,s^{-1}}$, and $\kappa_2 = 0.083\ \mathrm{cm^2\,s^{-1}}$. The thickness of the sample is $d = 0.055$ cm, and the area of the sample is $A = 0.49\ \mathrm{cm^2}$. The intensity of the 43.3-MeV analysis beam is $1.9 \times 10^{11}\ \mathrm{ions\,s^{-1}}$, which corresponds to an energy flux $F_0 = 2.7\ \mathrm{J\,s^{-1}\,cm^{-2}}$ when the beam spot size is equal to the sample area [models (a) and (b)] and $F_0 = 8.8\ \mathrm{J\,s^{-1}\,cm^{-2}}$ when the actual beam spot size is 0.15 $\mathrm{cm^2}$ [model (c)]. To gain insight into the dependence of the thermal contact on the relevant quantities, we used different values for the thermal conductance of the interface between silicon and stainless steel: $H = 1.1 \times 10^{-3}$, 1.1×10^{-2}, 1.1×10^{-1}, 1.1×10^{0}, and $1.1 \times 10^{1}\ \mathrm{J\,s^{-1}\,cm^{-2}\,K^{-1}}$. The equation for the temperature rise $\Delta T(x,t)$ for models (a) and (b) reads

$$\frac{\partial \Delta T(x,t)}{\partial t} = \kappa \frac{\partial^2 \Delta T(x,t)}{\partial x^2}, \tag{A2}$$

with the initial condition $\Delta T(x,t) = 0$ at time $t = 0$, and relevant values for κ.

(a) *Semi-infinite solid.* The situation of a semi-infinite solid with a flux F_0 at the absorbing surface ($x = 0$) is treated by Carslaw and Jaeger.[28] First, they solved the heat equation for the energy flux $F(x,t)$, from which they obtained the increase of temperature $\Delta T(x,t)$:

$$\Delta T(x,t) = \frac{2F_0}{k_1}\left[\sqrt{\frac{\kappa_1 t}{\pi}}\exp\left(-\frac{x^2}{4\kappa_1 t}\right) - \frac{1}{2}x\,\mathrm{erfc}\left(\frac{x}{2\sqrt{\kappa_1 t}}\right)\right]. \tag{A3}$$

The results in Fig. 6 show the time and depth dependence of the temperature increase. We observe that the distribution of the temperature increase over typical film and substrate dimensions (film thickness 300×10^{-7} cm, substrate thickness 0.055 cm, and surface area $0.7 \times 0.7\ \mathrm{cm^{-2}}$) may be regarded as homogeneous over the depth of the sample and is on the order of 20 K in 100 s. When thermal contact with the stainless-steel sample holder is lacking significant sample heating may occur. This we will discuss using model (b).

(b) *Two-component semi-infinite solid.* The boundary condition at the sample surface ($x = 0$) reads

$$-k_1 \left.\frac{\partial \Delta T(x,t)}{\partial x}\right|_{x=0} = F_0. \tag{A4}$$

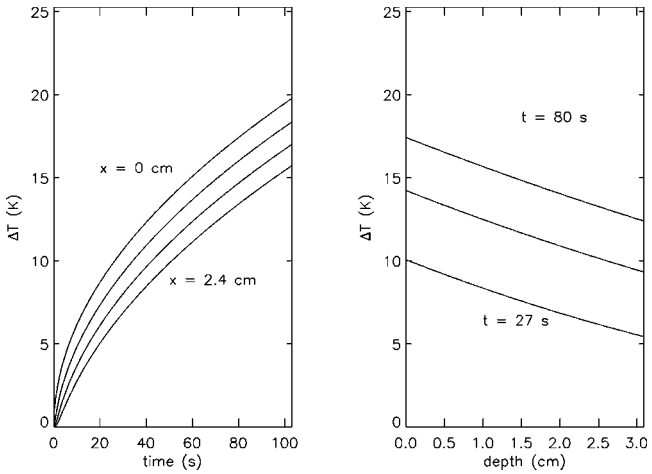

FIG. 6. The increase of the temperature of a *c*-Si sample caused by a 43.3-MeV Ag ion beam with an ion current of 1.9×10^{11} ions s^{-1}. The calculations were done for a sample with an infinite thickness and a surface of the size of the beam spot (0.15 cm^2). Both time and depth dependences are shown.

At the interface between silicon and the sample holder ($x=d$), the boundary conditions are given by

$$-k_1\left.\frac{\partial\Delta T(x,t)}{\partial x}\right|_{x\uparrow d}=-k_2\left.\frac{\partial\Delta T(x,t)}{\partial x}\right|_{x\downarrow d}, \tag{A5}$$

$$-k_1\left.\frac{\partial\Delta T(x,t)}{\partial x}\right|_{x\uparrow d}=H(\Delta T(x,t)|_{x\uparrow d}-\Delta T(x,t)|_{x\downarrow d}). \tag{A6}$$

These conditions express that the energy fluxes at both sides of the interface are equal, and that the flux is proportional to the thermal conductance H and the temperature difference over the interface. For practical reasons we define $\nu=k_1/Hd$ and $\sigma=k_2/k_1\sqrt{\kappa_1/\kappa_2}$. ν is a measure of the thermal resistance over the interface. Furthermore, we introduce the functions

$$\Omega(w,t)=\frac{2}{k_1\pi}\,\frac{1-\exp\left(\dfrac{-w^2t}{\tau}\right)}{w^2}, \tag{A7}$$

$$\Phi(w,x)=\frac{d\sigma\cos\left(\dfrac{wx}{l}\right)}{\sigma^2(\cos w-\nu w\sin w)^2+\sin^2 w}, \tag{A8}$$

$$\Sigma(w)=\frac{d\sigma w\sin w}{\sigma^2(\cos w-\nu w\sin w)^2+\sin^2 w}. \tag{A9}$$

In this model $\tau=d^2/\kappa_1(\tau=0.003\,\mathrm{s})$.

As for model (a), first we derive the energy flux $F(x,t)$, from which the temperature profile $\Delta T(x,t)$, the global temperature rise $\Delta T(t)$, and the temperature step $\Delta\Theta(t)$ at the interface ($x=d$) of silicon and stainless steel are obtained:

$$F(x,t)=-F_0k_1\int_0^\infty\Omega(w,t)\,\frac{\partial}{\partial x}\Phi(w,x)dw, \tag{A10}$$

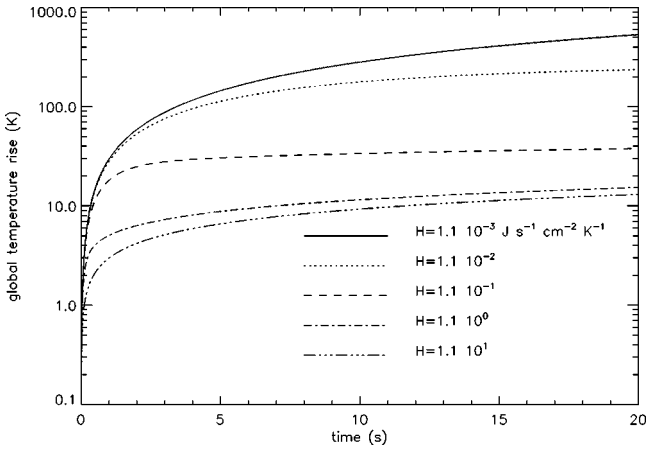

FIG. 7. The time dependence of the global temperature increase of a silicon sample on a stainless-steel substrate for different values of the thermal conductance H at the interface. The calculations were done for a silicon sample with a thickness of 0.055 cm and an area of 0.15 cm^2. The incoming energy flux is 8.8 J s^{-1} cm^{-2}.

$$\Delta T(x,t)=F_0\int_0^\infty\Omega(w,t)\Phi(w,x)dw \quad \text{for} \quad 0<x<d, \tag{A11}$$

$$\Delta T(t)=F_0\int_0^\infty\Omega(w,t)\,\frac{\Sigma(w)}{w^2}dw, \tag{A12}$$

$$\Delta\Theta(t)=F_0\nu\int_0^\infty\Omega(w,t)\Sigma(w)dw. \tag{A13}$$

It turns out that within the silicon the variation of the temperature rise is so small $[\Delta T(0,t)-\Delta T(0.055,t)<0.3\,\mathrm{K}]$ that one may restrict oneself to calculating the global temperature rise of the silicon. The time dependence of the global temperature increase and the temperature step at the interface between silicon and stainless steel are shown in Figs. 7 and 8 for different values of H. These results show that for lower values ($H<1.1\,\mathrm{J\,s^{-1}\,cm^{-2}\,K^{-1}}$) the thermal conductance H will strongly influence the temperature rise. For higher values the experimental conditions are not affected.

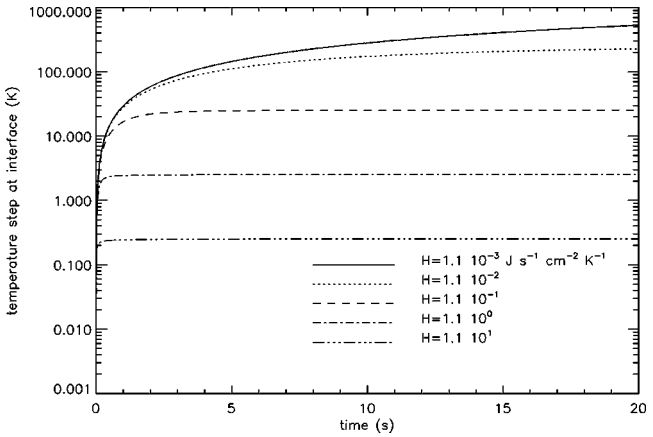

FIG. 8. The time dependence of the temperature step at the silicon stainless-steel interface for different values of the thermal conductance H.

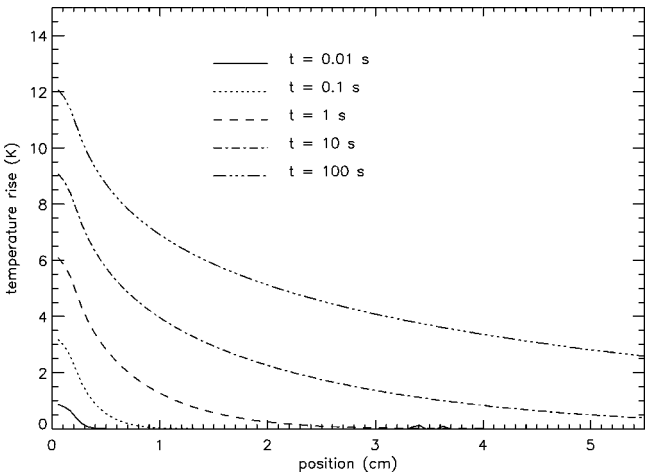

FIG. 9. The temperature rise of a 0.055-cm-thick silicon sample in the case when the incoming energy is dissipated in the plane of the sample surface. The sample is considered to be infinitely extended.

(c) *The lateral system*. The considered system consists of an infinitely extended plane of silicon in which a disk with the area of the beam spot (0.15 cm^2) and a thickness d absorbs the energy of the analyzing beam. The energy generation per unit of time and per unit of volume within the disk equals F_0/d. The material constants inside and outside of the disc are equal. By adapting the method of Carslaw and Jaeger[28] for treating the heat conduction in a cylinder, we obtained expressions for the temperature profile $T(r,t)$, the energy current $S(t)$ through the margin of the disk and its global temperature rise $\Delta T(t)$ (r is the distance to the center of the disk):

$$T(r,t)=\frac{F_0\pi a^2}{2d}\int_0^\infty \Omega(w,t)J0\left(\frac{wr}{a}\right)J1(w)dw, \tag{A14}$$

$$S(t)=k_1F_0\pi^2a^2\int_0^\infty w\Omega(w,t)J1(w)^2dw, \tag{A15}$$

$$\Delta T(t)=\frac{F_0\pi a^2}{d}\int_0^\infty \frac{\Omega(w,t)}{w}J1(w)^2dw, \tag{A16}$$

where $J0(w)$ and $J1(w)$ are Bessel functions, the radius of the beam spot $a=0.22$ cm, and $\tau=a^2/\kappa_1(\tau=0.052\,\mathrm{s})$. In Fig. 9 we show the temperature rise as a function of r for different values of time. This demonstrates that this rise is small compared to the results for the other models.

For the underlying models we also derived the asymptotic expressions ($t\to\infty, t\gg\tau$) for the (global) temperature increase of the sample ($x\leqslant d$). For the linear models one obtains

$$\text{(a)}\quad \Delta T(t)\approx\frac{2F_0d}{\sqrt{\pi}k_1}\sqrt{\frac{t}{\tau}}\quad\text{for}\quad t\gg\tau\quad\text{where}\quad\tau=\frac{d^2}{\kappa_1}, \tag{A17}$$

$$\text{(b)}\quad \Delta T(t)\approx\frac{2F_0d}{\sqrt{\pi}k_1\sigma}\sqrt{\frac{t}{\tau}}\quad\text{for}\quad t\gg\tau\quad\text{where}\quad\tau=\frac{d^2}{\kappa_1}, \tag{A18}$$

and, for the two-dimensional model,

$$\text{(c)}\quad \Delta T(t)\approx\frac{F_0a^2}{4k_1d}\ln\frac{t}{\tau}\quad\text{for}\quad t\gg\tau\quad\text{where}\quad\tau=\frac{a^2}{\kappa_1}. \tag{A19}$$

Because of the small value of τ [$\tau=0.003$ s for (a) and (b)], the graphs in Figs. 6 and 7 are fitted well with these functions with the exception of very small values of H.

The remaining difference between model (a) and (b) for large values of H is due to the presence of two different materials. This is controlled by σ in Eq. (A18).

From the two-dimensional situation we note that the heat is distributed over the sample area (0.49 cm^2) within seconds. Experiments in which we repeated the irradiation at an adjacent spot on the sample gave the same results. From this we conclude that, even after elongated irradiation, the material remains below the temperature where thermal release of hydrogen starts (300 °C). We use this result to calculate a lower limit for H. Requiring $\Delta T(t=250\,\mathrm{s})<300\,^\circ\mathrm{C}$ in model (b) we obtain $H>1.1\times10^{-2}$ $\mathrm{J\,s^{-1}\,cm^{-2}\,K^{-1}}$. This corresponds with the dotted line in Fig. 7. Most conclusions can be drawn on the basis of observations in the first few seconds after the start of the irradiation. So, finally, we derive that the upper limit for the temperature in the most important experimental regime is on the order of 50 °C.

From the models treated above we conclude that to reduce the heating of a sample one has to take care of sufficient thermal contact between the sample and its holder. Furthermore, it appears that heat is quickly distributed over silicon samples, even if their size exceeds several centimeters. This means that the dimensions of the sample are more important than the size of the beam spot.

[1] W. M. Arnoldbik and F. H. P. M. Habraken, Rep. Prog. Phys. **56**, 859 (1993).
[2] L. C. Feldman and J. W. Mayer, *Fundamentals of Surface and Thin Films Analysis* (Elsevier, New York, 1986).
[3] M. E. Adel, O. Amir, R. Kalish, and L. C. Feldman, J. Appl. Phys. **66**, 3248 (1989).
[4] C. H. M. Marée, A. M. Vredenberg, and F. H. P. M. Habraken, Mater. Chem. Phys. **46**, 198 (1996).
[5] M. P. de Jong, A. J. H. Maas, L. J. van IJzendoorn, S. S. Klein, and M. J. A. de Voigt, J. Appl. Phys. **82**, 1058 (1997).
[6] Y. J. Chabal and C. K. N. Patel, Rev. Mod. Phys. **59**, 835 (1987).
[7] W. Beyer, H. Wagner, and F. Finger, J. Non-Cryst. Solids **77&78**, 857 (1985).
[8] E. H. C. Ullersma, D. K. Inia, F. H. P. M. Habraken, W. G. J. H. M. van Sark, W. F. van der Weg, K. T. Westerduin, and A. van Veen, in *Amorphous and Microcrystalline Silicon Technology–1997*, edited by E. A. Schiff, M. Hack, S. Wagner, R. E. I. Schropp, and I. Shimizu, MRS Symposium Proceedings No. 467 (Materials Research Society, Pittsburgh, 1997), pp. 141–146.

[9] D. L. Staebler and C. R. Wronski, Appl. Phys. Lett. **31**, 292 (1977).
[10] F. Maass, J. Bertomeu, J. M. Asensi, J. Puigdollers, J. Andreu, J. C. Delgado, and J. Esteve, Appl. Surf. Sci. **70&71**, 768 (1993).
[11] D. L. Williamson, A. H. Mahan, B. P. Nelson, and R. S. Crandall, Appl. Phys. Lett. **55**, 783 (1989).
[12] T. Friessnegg, M. Boudreau, P. Mascher, A. Knights, P. J. Simpson, and W. Puff, J. Appl. Phys. **84**, 786 (1998).
[13] E. H. C. Ullersma, Ph.D. thesis, Utrecht University, 1998.
[14] W. Möller, P. Børgesen, and B. M. U. Scherzer, Nucl. Instrum. Methods Phys. Res. B **19/20**, 826 (1987).
[15] P. Görts, Ph.D. thesis, Utrecht University, 1995.
[16] C. A. M. Stap, H. Meiling, G. Landweer, J. Bezemer, and W. F. van der Weg, in *Proceedings of the Ninth E. C. Photovoltaic Solar Energy Conference*, F.R.G., 1989, edited by W. Palz, G. T. Wrixon, and P. Helm (Kluwer, Dordrecht, 1989), p. 74.
[17] J. F. Ziegler, J. P. Biersack, and U. Littmark, *The Stopping and Range of Ions in Solids* (Pergamon, New York, 1995).
[18] C. H. M. Marée, A. Kleinpenning, A. M. Vredenberg, and F. H. P. M. Habraken, Nucl. Instrum. Methods Phys. Res. B **118**, 118 (1996).
[19] E. T. Foley, A. F. Kam, and J. W. Lyding, Phys. Rev. Lett. **80**, 1336 (1998).
[20] R. Biswas, Y.-P. Li, and B. C. Pan, Appl. Phys. Lett. **72**, 3500 (1998).
[21] J. Chevallier, M. Barbé, E. Constant, D. Loridant-Bernard, and M. Constant, Appl. Phys. Lett. **75**, 112 (1999).
[22] G. V. d. Walle and W. B. Jackson, Appl. Phys. Lett. **69**, 2441 (1996).
[23] A. J. H. Maas, Ph.D. thesis, Eindhoven Technical University, 1998.
[24] J. Perrin, M. Shiratani, P. Kae-Nune, H. Videlot, J. Jolly, and J. Guillon, J. Vac. Sci. Technol. A **16**, 278 (1998).
[25] Y. Muramatsu and N. Yabumoto, Appl. Phys. Lett. **49**, 1230 (1986).
[26] P. Kae-Nune, J. Perrin, J. Guillon, and J. Jolly, Plasma Sources Sci. Technol. **4**, 250 (1995).
[27] E. H. C. Ullersma, P. Ullersma, and F. H. P. M. Habraken (unpublished).
[28] H. S. Carslaw and J. C. Jaeger, *Conduction of Heat in Solids*, 2nd ed. (Clarendon Press, Oxford, 1959), Chap. II, p. 75.